BABAR-CONF-04/32
SLAC-PUB-10643
hep-ex/0408065
August 2004

Measurement of the $B^0 \to K^0_s K^0_s K^0_s$ Branching Fraction

The *BABAR* Collaboration

August 16, 2004

Abstract

We report a preliminary measurement of the branching fraction for the decay $B^0 \to K^0_s K^0_s K^0_s$, where the K^0_s mesons are reconstructed through the decay $K^0_s \to \pi^+\pi^-$. The measurement was performed on a sample of 211×10^6 $B\overline{B}$ pairs collected by the *BABAR* detector running on the $\Upsilon(4S)$ resonance at the PEP-II storage ring. The branching fraction is measured to be

$$\mathcal{B}(B^0 \to K^0_s K^0_s K^0_s) = (6.5 \pm 0.8 \pm 0.8) \times 10^{-6},$$

where the errors are statistical and systematic, respectively.

Submitted to the 32nd International Conference on High-Energy Physics, ICHEP 04,
16 August—22 August 2004, Beijing, China

Stanford Linear Accelerator Center, Stanford University, Stanford, CA 94309

Work supported in part by Department of Energy contract DE-AC03-76SF00515.

The *BABAR* Collaboration,

B. Aubert, R. Barate, D. Boutigny, F. Couderc, J.-M. Gaillard, A. Hicheur, Y. Karyotakis, J. P. Lees, V. Tisserand, A. Zghiche

Laboratoire de Physique des Particules, F-74941 Annecy-le-Vieux, France

A. Palano, A. Pompili

Università di Bari, Dipartimento di Fisica and INFN, I-70126 Bari, Italy

J. C. Chen, N. D. Qi, G. Rong, P. Wang, Y. S. Zhu

Institute of High Energy Physics, Beijing 100039, China

G. Eigen, I. Ofte, B. Stugu

University of Bergen, Inst. of Physics, N-5007 Bergen, Norway

G. S. Abrams, A. W. Borgland, A. B. Breon, D. N. Brown, J. Button-Shafer, R. N. Cahn, E. Charles, C. T. Day, M. S. Gill, A. V. Gritsan, Y. Groysman, R. G. Jacobsen, R. W. Kadel, J. Kadyk, L. T. Kerth, Yu. G. Kolomensky, G. Kukartsev, G. Lynch, L. M. Mir, P. J. Oddone, T. J. Orimoto, M. Pripstein, N. A. Roe, M. T. Ronan, V. G. Shelkov, W. A. Wenzel

Lawrence Berkeley National Laboratory and University of California, Berkeley, CA 94720, USA

M. Barrett, K. E. Ford, T. J. Harrison, A. J. Hart, C. M. Hawkes, S. E. Morgan, A. T. Watson

University of Birmingham, Birmingham, B15 2TT, United Kingdom

M. Fritsch, K. Goetzen, T. Held, H. Koch, B. Lewandowski, M. Pelizaeus, M. Steinke

Ruhr Universität Bochum, Institut für Experimentalphysik 1, D-44780 Bochum, Germany

J. T. Boyd, N. Chevalier, W. N. Cottingham, M. P. Kelly, T. E. Latham, F. F. Wilson

University of Bristol, Bristol BS8 1TL, United Kingdom

T. Cuhadar-Donszelmann, C. Hearty, N. S. Knecht, T. S. Mattison, J. A. McKenna, D. Thiessen

University of British Columbia, Vancouver, BC, Canada V6T 1Z1

A. Khan, P. Kyberd, L. Teodorescu

Brunel University, Uxbridge, Middlesex UB8 3PH, United Kingdom

A. E. Blinov, V. E. Blinov, V. P. Druzhinin, V. B. Golubev, V. N. Ivanchenko, E. A. Kravchenko, A. P. Onuchin, S. I. Serednyakov, Yu. I. Skovpen, E. P. Solodov, A. N. Yushkov

Budker Institute of Nuclear Physics, Novosibirsk 630090, Russia

D. Best, M. Bruinsma, M. Chao, I. Eschrich, D. Kirkby, A. J. Lankford, M. Mandelkern, R. K. Mommsen, W. Roethel, D. P. Stoker

University of California at Irvine, Irvine, CA 92697, USA

C. Buchanan, B. L. Hartfiel

University of California at Los Angeles, Los Angeles, CA 90024, USA

S. D. Foulkes, J. W. Gary, B. C. Shen, K. Wang

University of California at Riverside, Riverside, CA 92521, USA

D. del Re, H. K. Hadavand, E. J. Hill, D. B. MacFarlane, H. P. Paar, Sh. Rahatlou, V. Sharma

University of California at San Diego, La Jolla, CA 92093, USA

J. W. Berryhill, C. Campagnari, B. Dahmes, O. Long, A. Lu, M. A. Mazur, J. D. Richman, W. Verkerke

University of California at Santa Barbara, Santa Barbara, CA 93106, USA

T. W. Beck, A. M. Eisner, C. A. Heusch, J. Kroseberg, W. S. Lockman, G. Nesom, T. Schalk, B. A. Schumm, A. Seiden, P. Spradlin, D. C. Williams, M. G. Wilson

University of California at Santa Cruz, Institute for Particle Physics, Santa Cruz, CA 95064, USA

J. Albert, E. Chen, G. P. Dubois-Felsmann, A. Dvoretskii, D. G. Hitlin, I. Narsky, T. Piatenko, F. C. Porter, A. Ryd, A. Samuel, S. Yang

California Institute of Technology, Pasadena, CA 91125, USA

S. Jayatilleke, G. Mancinelli, B. T. Meadows, M. D. Sokoloff

University of Cincinnati, Cincinnati, OH 45221, USA

T. Abe, F. Blanc, P. Bloom, S. Chen, W. T. Ford, U. Nauenberg, A. Olivas, P. Rankin, J. G. Smith, J. Zhang, L. Zhang

University of Colorado, Boulder, CO 80309, USA

A. Chen, J. L. Harton, A. Soffer, W. H. Toki, R. J. Wilson, Q. Zeng

Colorado State University, Fort Collins, CO 80523, USA

D. Altenburg, T. Brandt, J. Brose, M. Dickopp, E. Feltresi, A. Hauke, H. M. Lacker, R. Müller-Pfefferkorn, R. Nogowski, S. Otto, A. Petzold, J. Schubert, K. R. Schubert, R. Schwierz, B. Spaan, J. E. Sundermann

Technische Universität Dresden, Institut für Kern- und Teilchenphysik, D-01062 Dresden, Germany

D. Bernard, G. R. Bonneaud, F. Brochard, P. Grenier, S. Schrenk, Ch. Thiebaux, G. Vasileiadis, M. Verderi

Ecole Polytechnique, LLR, F-91128 Palaiseau, France

D. J. Bard, P. J. Clark, D. Lavin, F. Muheim, S. Playfer, Y. Xie

University of Edinburgh, Edinburgh EH9 3JZ, United Kingdom

M. Andreotti, V. Azzolini, D. Bettoni, C. Bozzi, R. Calabrese, G. Cibinetto, E. Luppi, M. Negrini, L. Piemontese, A. Sarti

Università di Ferrara, Dipartimento di Fisica and INFN, I-44100 Ferrara, Italy

E. Treadwell

Florida A&M University, Tallahassee, FL 32307, USA

F. Anulli, R. Baldini-Ferroli, A. Calcaterra, R. de Sangro, G. Finocchiaro, P. Patteri, I. M. Peruzzi, M. Piccolo, A. Zallo

Laboratori Nazionali di Frascati dell'INFN, I-00044 Frascati, Italy

A. Buzzo, R. Capra, R. Contri, G. Crosetti, M. Lo Vetere, M. Macri, M. R. Monge, S. Passaggio, C. Patrignani, E. Robutti, A. Santroni, S. Tosi

Università di Genova, Dipartimento di Fisica and INFN, I-16146 Genova, Italy

S. Bailey, G. Brandenburg, K. S. Chaisanguanthum, M. Morii, E. Won

Harvard University, Cambridge, MA 02138, USA

R. S. Dubitzky, U. Langenegger

Universität Heidelberg, Physikalisches Institut, Philosophenweg 12, D-69120 Heidelberg, Germany

W. Bhimji, D. A. Bowerman, P. D. Dauncey, U. Egede, J. R. Gaillard, G. W. Morton, J. A. Nash, M. B. Nikolich, G. P. Taylor

Imperial College London, London, SW7 2AZ, United Kingdom

M. J. Charles, G. J. Grenier, U. Mallik

University of Iowa, Iowa City, IA 52242, USA

J. Cochran, H. B. Crawley, J. Lamsa, W. T. Meyer, S. Prell, E. I. Rosenberg, A. E. Rubin, J. Yi

Iowa State University, Ames, IA 50011-3160, USA

M. Biasini, R. Covarelli, M. Pioppi

Università di Perugia, Dipartimento di Fisica and INFN, I-06100 Perugia, Italy

M. Davier, X. Giroux, G. Grosdidier, A. Höcker, S. Laplace, F. Le Diberder, V. Lepeltier, A. M. Lutz, T. C. Petersen, S. Plaszczynski, M. H. Schune, L. Tantot, G. Wormser

Laboratoire de l'Accélérateur Linéaire, F-91898 Orsay, France

C. H. Cheng, D. J. Lange, M. C. Simani, D. M. Wright

Lawrence Livermore National Laboratory, Livermore, CA 94550, USA

A. J. Bevan, C. A. Chavez, J. P. Coleman, I. J. Forster, J. R. Fry, E. Gabathuler, R. Gamet, D. E. Hutchcroft, R. J. Parry, D. J. Payne, R. J. Sloane, C. Touramanis

University of Liverpool, Liverpool L69 72E, United Kingdom

J. J. Back,[1] C. M. Cormack, P. F. Harrison,[1] F. Di Lodovico, G. B. Mohanty[1]

Queen Mary, University of London, E1 4NS, United Kingdom

C. L. Brown, G. Cowan, R. L. Flack, H. U. Flaecher, M. G. Green, P. S. Jackson, T. R. McMahon, S. Ricciardi, F. Salvatore, M. A. Winter

University of London, Royal Holloway and Bedford New College, Egham, Surrey TW20 0EX, United Kingdom

D. Brown, C. L. Davis

University of Louisville, Louisville, KY 40292, USA

J. Allison, N. R. Barlow, R. J. Barlow, P. A. Hart, M. C. Hodgkinson, G. D. Lafferty, A. J. Lyon, J. C. Williams

University of Manchester, Manchester M13 9PL, United Kingdom

A. Farbin, W. D. Hulsbergen, A. Jawahery, D. Kovalskyi, C. K. Lae, V. Lillard, D. A. Roberts

University of Maryland, College Park, MD 20742, USA

G. Blaylock, C. Dallapiccola, K. T. Flood, S. S. Hertzbach, R. Kofler, V. B. Koptchev, T. B. Moore, S. Saremi, H. Staengle, S. Willocq

University of Massachusetts, Amherst, MA 01003, USA

[1]Now at Department of Physics, University of Warwick, Coventry, United Kingdom

R. Cowan, G. Sciolla, S. J. Sekula, F. Taylor, R. K. Yamamoto

Massachusetts Institute of Technology, Laboratory for Nuclear Science, Cambridge, MA 02139, USA

D. J. J. Mangeol, P. M. Patel, S. H. Robertson

McGill University, Montréal, QC, Canada H3A 2T8

A. Lazzaro, V. Lombardo, F. Palombo

Università di Milano, Dipartimento di Fisica and INFN, I-20133 Milano, Italy

J. M. Bauer, L. Cremaldi, V. Eschenburg, R. Godang, R. Kroeger, J. Reidy, D. A. Sanders, D. J. Summers, H. W. Zhao

University of Mississippi, University, MS 38677, USA

S. Brunet, D. Côté, P. Taras

Université de Montréal, Laboratoire René J. A. Lévesque, Montréal, QC, Canada H3C 3J7

H. Nicholson

Mount Holyoke College, South Hadley, MA 01075, USA

N. Cavallo,[2] F. Fabozzi,[2] C. Gatto, L. Lista, D. Monorchio, P. Paolucci, D. Piccolo, C. Sciacca

Università di Napoli Federico II, Dipartimento di Scienze Fisiche and INFN, I-80126, Napoli, Italy

M. Baak, H. Bulten, G. Raven, H. L. Snoek, L. Wilden

NIKHEF, National Institute for Nuclear Physics and High Energy Physics, NL-1009 DB Amsterdam, The Netherlands

C. P. Jessop, J. M. LoSecco

University of Notre Dame, Notre Dame, IN 46556, USA

T. Allmendinger, K. K. Gan, K. Honscheid, D. Hufnagel, H. Kagan, R. Kass, T. Pulliam, A. M. Rahimi, R. Ter-Antonyan, Q. K. Wong

Ohio State University, Columbus, OH 43210, USA

J. Brau, R. Frey, O. Igonkina, C. T. Potter, N. B. Sinev, D. Strom, E. Torrence

University of Oregon, Eugene, OR 97403, USA

F. Colecchia, A. Dorigo, F. Galeazzi, M. Margoni, M. Morandin, M. Posocco, M. Rotondo, F. Simonetto, R. Stroili, G. Tiozzo, C. Voci

Università di Padova, Dipartimento di Fisica and INFN, I-35131 Padova, Italy

M. Benayoun, H. Briand, J. Chauveau, P. David, Ch. de la Vaissière, L. Del Buono, O. Hamon, M. J. J. John, Ph. Leruste, J. Malcles, J. Ocariz, M. Pivk, L. Roos, S. T'Jampens, G. Therin

Universités Paris VI et VII, Laboratoire de Physique Nucléaire et de Hautes Energies, F-75252 Paris, France

P. F. Manfredi, V. Re

Università di Pavia, Dipartimento di Elettronica and INFN, I-27100 Pavia, Italy

[2]Also with Università della Basilicata, Potenza, Italy

P. K. Behera, L. Gladney, Q. H. Guo, J. Panetta

University of Pennsylvania, Philadelphia, PA 19104, USA

C. Angelini, G. Batignani, S. Bettarini, M. Bondioli, F. Bucci, G. Calderini, M. Carpinelli, F. Forti, M. A. Giorgi, A. Lusiani, G. Marchiori, F. Martinez-Vidal,[3] M. Morganti, N. Neri, E. Paoloni, M. Rama, G. Rizzo, F. Sandrelli, J. Walsh

Università di Pisa, Dipartimento di Fisica, Scuola Normale Superiore and INFN, I-56127 Pisa, Italy

M. Haire, D. Judd, K. Paick, D. E. Wagoner

Prairie View A&M University, Prairie View, TX 77446, USA

N. Danielson, P. Elmer, Y. P. Lau, C. Lu, V. Miftakov, J. Olsen, A. J. S. Smith, A. V. Telnov

Princeton University, Princeton, NJ 08544, USA

F. Bellini, G. Cavoto,[4] R. Faccini, F. Ferrarotto, F. Ferroni, M. Gaspero, L. Li Gioi, M. A. Mazzoni, S. Morganti, M. Pierini, G. Piredda, F. Safai Tehrani, C. Voena

Università di Roma La Sapienza, Dipartimento di Fisica and INFN, I-00185 Roma, Italy

S. Christ, G. Wagner, R. Waldi

Universität Rostock, D-18051 Rostock, Germany

T. Adye, N. De Groot, B. Franek, N. I. Geddes, G. P. Gopal, E. O. Olaiya

Rutherford Appleton Laboratory, Chilton, Didcot, Oxon, OX11 0QX, United Kingdom

R. Aleksan, S. Emery, A. Gaidot, S. F. Ganzhur, P.-F. Giraud, G. Hamel de Monchenault, W. Kozanecki, M. Legendre, G. W. London, B. Mayer, G. Schott, G. Vasseur, Ch. Yèche, M. Zito

DSM/Dapnia, CEA/Saclay, F-91191 Gif-sur-Yvette, France

M. V. Purohit, A. W. Weidemann, J. R. Wilson, F. X. Yumiceva

University of South Carolina, Columbia, SC 29208, USA

D. Aston, R. Bartoldus, N. Berger, A. M. Boyarski, O. L. Buchmueller, R. Claus, M. R. Convery, M. Cristinziani, G. De Nardo, D. Dong, J. Dorfan, D. Dujmic, W. Dunwoodie, E. E. Elsen, S. Fan, R. C. Field, T. Glanzman, S. J. Gowdy, T. Hadig, V. Halyo, C. Hast, T. Hryn'ova, W. R. Innes, M. H. Kelsey, P. Kim, M. L. Kocian, D. W. G. S. Leith, J. Libby, S. Luitz, V. Luth, H. L. Lynch, H. Marsiske, R. Messner, D. R. Muller, C. P. O'Grady, V. E. Ozcan, A. Perazzo, M. Perl, S. Petrak, B. N. Ratcliff, A. Roodman, A. A. Salnikov, R. H. Schindler, J. Schwiening, G. Simi, A. Snyder, A. Soha, J. Stelzer, D. Su, M. K. Sullivan, J. Va'vra, S. R. Wagner, M. Weaver, A. J. R. Weinstein, W. J. Wisniewski, M. Wittgen, D. H. Wright, A. K. Yarritu, C. C. Young

Stanford Linear Accelerator Center, Stanford, CA 94309, USA

P. R. Burchat, A. J. Edwards, T. I. Meyer, B. A. Petersen, C. Roat

Stanford University, Stanford, CA 94305-4060, USA

S. Ahmed, M. S. Alam, J. A. Ernst, M. A. Saeed, M. Saleem, F. R. Wappler

State University of New York, Albany, NY 12222, USA

[3]Also with IFIC, Instituto de Física Corpuscular, CSIC-Universidad de Valencia, Valencia, Spain
[4]Also with Princeton University, Princeton, USA

W. Bugg, M. Krishnamurthy, S. M. Spanier
University of Tennessee, Knoxville, TN 37996, USA

R. Eckmann, H. Kim, J. L. Ritchie, A. Satpathy, R. F. Schwitters
University of Texas at Austin, Austin, TX 78712, USA

J. M. Izen, I. Kitayama, X. C. Lou, S. Ye
University of Texas at Dallas, Richardson, TX 75083, USA

F. Bianchi, M. Bona, F. Gallo, D. Gamba
Università di Torino, Dipartimento di Fisica Sperimentale and INFN, I-10125 Torino, Italy

L. Bosisio, C. Cartaro, F. Cossutti, G. Della Ricca, S. Dittongo, S. Grancagnolo, L. Lanceri, P. Poropat,[5] L. Vitale, G. Vuagnin
Università di Trieste, Dipartimento di Fisica and INFN, I-34127 Trieste, Italy

R. S. Panvini
Vanderbilt University, Nashville, TN 37235, USA

Sw. Banerjee, C. M. Brown, D. Fortin, P. D. Jackson, R. Kowalewski, J. M. Roney, R. J. Sobie
University of Victoria, Victoria, BC, Canada V8W 3P6

H. R. Band, B. Cheng, S. Dasu, M. Datta, A. M. Eichenbaum, M. Graham, J. J. Hollar, J. R. Johnson, P. E. Kutter, H. Li, R. Liu, A. Mihalyi, A. K. Mohapatra, Y. Pan, R. Prepost, P. Tan, J. H. von Wimmersperg-Toeller, J. Wu, S. L. Wu, Z. Yu
University of Wisconsin, Madison, WI 53706, USA

M. G. Greene, H. Neal
Yale University, New Haven, CT 06511, USA

[5]Deceased

1 INTRODUCTION

In this paper we report a measurement of the branching fraction ($\mathcal{B}$) for $B^0 \to K^0_s K^0_s K^0_s$. This decay is expected to be penguin dominated; the simplest diagram that can be drawn without rescattering is shown in Fig. 1. $B^0 \to K^0_s K^0_s K^0_s$ is *not* Cabibbo-suppressed, and so is expected to have substantially larger branching fraction than $B^0 \to 2K^0_s$.

In Ref. [1] the branching fraction $\mathcal{B}(B^0 \to K^0_s K^0_s K^0_s)$ is related to $\mathcal{B}(B^+ \to K^+K^-K^+)$. With the assumption of gluonic penguin dominance and the usual assumption $\mathcal{B}(K^0 \to K^0_s) = \mathcal{B}(\overline{K}^0 \to K^0_s) = 0.5$, they derive $\mathcal{B}(B^+ \to K^+K^-K^+) = \mathcal{B}(B^0 \to K^0\overline{K}^0) = 8\mathcal{B}(B^0 \to K^0_s K^0_s K^0_s)$. Using the *BABAR* and Belle averaged value [2] of $\mathcal{B}(B^+ \to K^+K^-K^+) = (29.5 \pm 1.8) \times 10^{-6}$, $\mathcal{B}(B^0 \to K^0_s K^0_s K^0_s)$ is expected to be $\sim 4 \times 10^{-6}$.

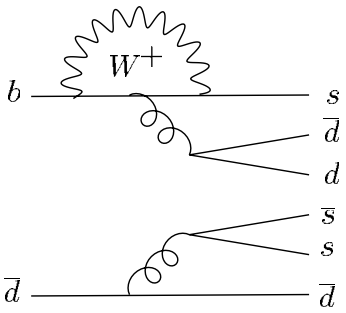

Figure 1: The dominant diagram for the decay $B^0 \to K^0_s K^0_s K^0_s$.

The only previous measurement [3] of this branching fraction is from the Belle Collaboration, $\mathcal{B}(B^0 \to K^0_s K^0_s K^0_s) = (4.2^{+1.6}_{-1.3} \pm 0.8) \times 10^{-6}$, based on 78 fb^{-1} of on-resonance data. The data sample used in this paper is 2.7 the size of that data sample, and the $B^0 \to K^0_s K^0_s K^0_s$ efficiency we estimate for our analysis is larger than that in Ref. [3].

In this paper we report an inclusive measurement of $B^0 \to K^0_s K^0_s K^0_s$. In addition to non-resonant three-body $b \to s\overline{q}q$, ($\overline{q}q = \overline{s}s$ or $\overline{d}d$) gluonic penguin decays, charmless resonant intermediate states like $B^0 \to f_0 K^0$ can produce the $3K^0_s$ final state. There may also be $b \to c\overline{c}s$ decays that lead to the $3K^0_s$ final state. The dominant of these is expected to be $B^0 \to \chi_{c0} K^0 \to 3K^0_s$, but its product branching fraction [4] is $< 0.5 \times 10^{-6}$ (90% CL), about a factor of ten smaller than that expected for $B^0 \to K^0_s K^0_s K^0_s$. We do not exclude these from this measurement, though we will do a search for $B^0 \to \chi_{c0} K^0_s$ as a systematic check. The product branching fraction for $B^0 \to \overline{D}^0 K^0 \to 3K^0_s$ is estimated [4] to be $\sim 9 \times 10^{-9}$ and therefore will be ignored.

2 THE *BABAR* DETECTOR AND DATASET

The data used in this analysis were collected with the *BABAR* detector at the PEP-II storage ring. We use 191 fb^{-1} of data taken at the center-of-mass (CM) energy of the $\Upsilon(4S)$ resonance (the on-resonance data sample). These data correspond to 211×10^6 $B\overline{B}$ pairs.

The *BABAR* detector is described elsewhere [5]. The important parts of the detector for this analysis are the charged particle tracking detectors. These consist of five layers of double-sided silicon-strip detectors between the beampipe and a 40-layer cylindrical drift chamber, with both axial and

small-stereo-angle superlayers. Both detectors are in a 1.5 T solenoidal magnetic field, and provide excellent pattern recognition and momentum measurement for reconstruction of $K^0_s \to \pi^+\pi^-$ decays. The electromagnetic calorimeter also contributes to this analysis through the reconstruction of neutral particles which are used along with charged tracks not coming from the candidate $B^0 \to K^0_s K^0_s K^0_s$ decay to form continuum rejection variables.

Large samples of Monte Carlo (MC) simulated events are used throughout this analysis, to estimate the reconstruction efficiency and to derive parameters used to describe the signal and background (BG) shapes in the fit for the signal yield. Except for some parametrized MC samples used to validate the fit, all the MC samples were generated with GEANT4 [6], with the full detector-response simulation, and reconstructed with the same programs used for data reconstruction.

3 CANDIDATE SELECTION

3.1 K^0_s RECONSTRUCTION

All K^0_s candidates used in this analysis are reconstructed through the decay $K^0_s \to \pi^+\pi^-$. Every pair of oppositely-charged tracks that pass a very loose mass selection is fitted to a vertex. All pairs that pass a cut on the vertex-fit mass ($\Delta m_{\pi^+\pi^-} = |m_{\pi^+\pi^-} - m_{K^0_s}| < 10.8$ MeV) and a very loose vertex-fit χ^2 probability cut ($P(\chi^2) > 10^{-6}$) are retained for further consideration. Several more cuts are applied to the K^0_s candidates to reject combinatorial background and K^0_s mesons that are not B decay products. We require the transverse decay-length $r_{DEC} = \sqrt{(x_{K^0_s} - x_{BS})^2 + (y_{K^0_s} - y_{BS})^2}$ be between 0.2 and 40.0 cm. Here K^0_s refers to the fitted vertex position and BS refers to the position of the beamspot (the center of the luminous region), which is determined in *BABAR* approximately every ten minutes. The inner r_{DEC} requirement removes random $\pi^+\pi^-$ combinations that most likely come from a common point (the event primary vertex or a short-lived secondary decay) and just happen to have a mass inside the allowed $\Delta m_{\pi^+\pi^-}$ range. Candidates that fail the outer r_{DEC} criteria tend to be from calorimeter splash-back tracks that once again just happen to pass the $\Delta m_{\pi^+\pi^-}$ cut. We also require that the angle between the transverse flight vector (of which r_{DEC} is the magnitude) and the transverse momentum vector of the K^0_s be less than 200 mrad. These cuts, along with the continuum rejection criteria described below, have been optimized in a signal-blind study to produce the largest significance for a branching fraction measurement. The cuts were optimized using signal MC to represent the $B^0 \to K^0_s K^0_s K^0_s$ decay, and on-resonance data in mass sidebands, designed to exclude all signal candidates, to model backgrounds in the signal $m(K^0_s K^0_s K^0_s)$ region.

3.2 B^0 RECONSTRUCTION

All combinations of three $K^0_s \to \pi^+\pi^-$ candidates, where none of the candidates share a charged track, are used to form $B^0 \to K^0_s K^0_s K^0_s$ candidates. The K^0_s momentum is calculated in the $\pi^+\pi^-$ vertex fit, but because $m_{\pi^+\pi^-}$ is not constrained to $m_{K^0_s}$ in the vertex fit, we use $E_{K^0_s} = \sqrt{\vec{p}^{\,2}_{\pi^+\pi^-} + m^2_{K^0_s}}$ in place of the K^0_s energy.

We use two kinematic variables to separate the $B^0 \to K^0_s K^0_s K^0_s$ signal from backgrounds. The energy difference $\Delta E = E_B - \sqrt{s}/2$ is reconstructed from the energy of the B candidate in the e^+e^- CM frame E_B and the total energy $\sqrt{s}$. The ΔE mean value is expected to be near zero for signal events, and the ΔE resolution for signal events is about 18 MeV. The beam-energy-substituted mass is defined by $m_{\rm ES} = \sqrt{(s/2 + \vec{p}_i \cdot \vec{p}_B)^2/E_i^2 - \vec{p}_B^{\,2}}$, where $(\vec{p}_i, E_i)$ is the four-momentum of the

initial-state e^+e^- system and $\vec{p}_B$ is the momentum of the B candidate, both measured in the laboratory frame. The $m_{\rm ES}$ resolution for signal events is about 2.6 MeV. We retain candidates with $|\Delta E| < 0.30$ GeV and $5.22 < m_{\rm ES} < 5.30$ GeV (this is referred to as the bounded ΔE-$m_{\rm ES}$ plane).

Studies of off-resonance data and MC samples have shown that the largest background source that passes the above cuts comes from continuum $e^+e^- \to u\overline{u}/d\overline{d}/s\overline{s}/c\overline{c}$ events. For this reason we choose to cut on three variables that are commonly used to reject continuum background. The most powerful continuum-rejection cut is $|\cos\theta_T| < 0.8$, where $\cos\theta_T$ is the cosine of the angle between the B candidate thrust axis and the thrust axis of the remaining charged tracks and photons in the event. The $|\cos\theta_T|$ distribution is fairly uniform for signal events, and is peaked near 1 for continuum events. We also require $-5.0 < \mathcal{F} < +1.0$, where $\mathcal{F}$ is a Fisher discriminant [7] based on zeroth and second momentum-weighted Legendre polynomial sums of the remaining tracks and photons ($\mathcal{F} = 0.5264 - 0.1882\mathcal{L}_0 + 0.9417\mathcal{L}_2$), and $R_2 < 0.3$, where R_2 is the ratio of second to zeroth Fox-Wolfram moments [8].

After all the above cuts are applied, there are a small ($< 1\%$) number of events with more than one $3K_s^0$ candidate per event. While the MC appears to properly model this effect, we choose to simplify the analysis by using only the candidate with the smallest $\Sigma(\Delta m^i_{\pi^+\pi^-})^2$ in each event, where the sum is over the three K_s^0 candidates making up the $B^0 \to K_s^0K_s^0K_s^0$ candidate.

4 MAXIMUM LIKELIHOOD FIT FOR YIELD

We take all the combinations that pass the above cuts and extract the yield of signal $B^0 \to K_s^0K_s^0K_s^0$ events (N_S) with an unbinned extended maximum likelihood (ML) fit, where the likelihood is:

$$\mathcal{L} = \exp\left(-\sum_i N_i\right) \prod_{j=1} \left[\sum_i N_i \mathcal{P}_{ij}\right], \tag{1}$$

the sum over i corresponds to four categories of signal and background, the product over j corresponds to the 508 $B^0 \to K_s^0K_s^0K_s^0$ candidates that pass all the requirements in the previous section, and $\mathcal{P}_{ij}$ is the probability density function (PDF) for the ith category evaluated for the jth candidate. The PDFs used for the four components of the fit are described in the next sections. For all except one category, the PDFs are the products of one-dimensional PDFs in $m_{\rm ES}$ and ΔE:

$$\mathcal{P}_i = \mathcal{P}_i(m_{ES})\mathcal{P}_i(\Delta E).$$

The four categories whose yields N_i are determined by the fit are the above-mentioned number of signal events N_S, the number of continuum BG events N_{CBG}, the number of $B\overline{B}$ events in which the candidate comes from random combinations of tracks that may or many not be true $K_s^0 \to \pi^+\pi^-$ decays (the "non-peaking" $B\overline{B}$ BG) N_{BNOP}, and events where the three K_s^0 candidates come from the same B decay but that B decay is not a signal $B^0 \to K_s^0K_s^0K_s^0$ decay (the "peaking" BG) N_{BPBG}. The default fit requires all $N_i \geq 0$, but we loosen this requirement as a systematic cross-check, and see that the signal yield changes by a small amount.

The dominant source of peaking BG in the part of the ΔE-$m_{\rm ES}$ plane over which we do our fit is $B \to 3K_s^0\pi$ decays, where the π^+ or π^0 is missed. Many of the B branching fractions for decays that contribute to this background are known poorly or not at all [4], including the decays $B^0 \to 2K_s^0K^{*0}$ and $B^+ \to 2K_s^0K^{*+}$, which should dominate the peaking BG in the bounded ΔE-$m_{\rm ES}$ plane. Like the signal $B^0 \to K_s^0K_s^0K_s^0$ events, we remove the peaking BG from the generic

$B\overline{B}$ MC before we fit it to extract the parameters used to describe the non-peaking $B\overline{B}$ BG PDF. We generate large MC samples with only $B\overline{B}$ peaking BG, extract the peaking PDF from these samples, and allow the $B\overline{B}$ peaking and non-peaking yields to float separately. One reason the $|\Delta E|$ cut is so wide (< 300 MeV) on the bounded ΔE-$m_{\rm ES}$ plane is to allow a large enough region to fit the peaking BG. We do not attempt to extract a branching fraction for the peaking $B\overline{B}$ BG; our goal is to determine the size and shape of the peaking BG, so that its presence at an unexpectedly large level does not distort the shape of the non-peaking $B\overline{B}$ BG and lead to a systematic bias on N_S. It turns out that the fit to the data requires very little peaking *or* non-peaking $B\overline{B}$ BG, and the signal yield is changed negligibly if either or *both* of these populations are fixed at zero.

4.1 SIGNAL EFFICIENCY AND PROBABILITY DENSITY FUNCTION FOR SIGNAL

The signal PDF parameters are determined from ML fits to reconstructed and selected signal MC events from a sample of 148k generated $B^0 \to K^0_s K^0_s K^0_s$ decays. The signal distribution in ΔE is well described by a double-Gaussian (one for the "core," another for the broader "tail"). The five parameters that describe this double-Gaussian PDF are shown in Table 1. The signal PDF in m_{ES} is well described by a bifurcated Gaussian. The values of the three parameters determined from the fit to the signal MC are also shown in Table 1. Histograms of the signal MC, with the derived PDFs shown as overlaid curves, are shown in Fig. 2. A fit to the signal MC with these parameters gives a signal yield of $N_S = 8147 \pm 91$ events, or a signal efficiency of $(5.50 \pm 0.06)\%$.

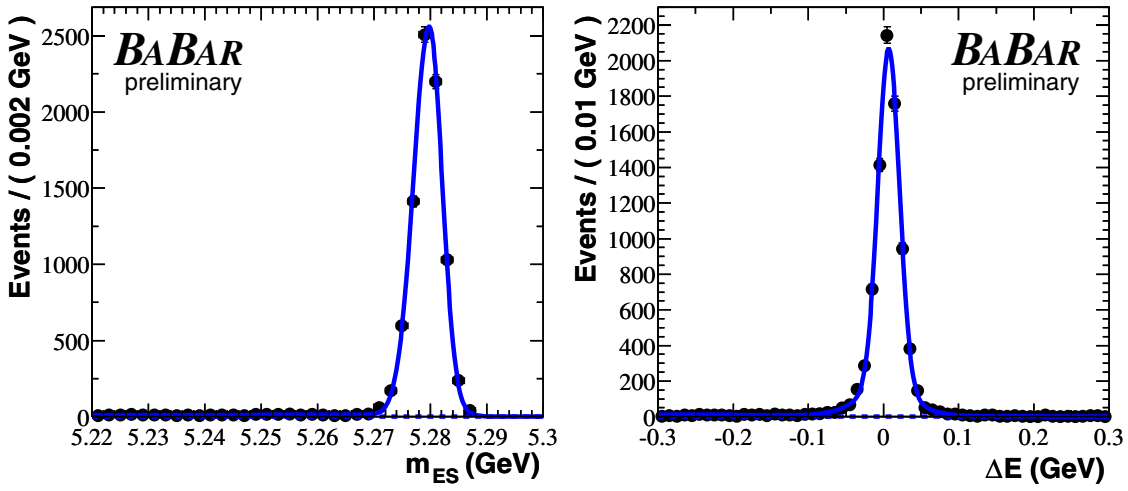

Figure 2: Distributions of m_{ES} and ΔE for selected candidates from MC simulated $B^0 \to K^0_s K^0_s K^0_s$ events. The curves overlaid on the MC data points are the signal PDFs determined from a unbinned fit. The parameters from the fit are shown in Table 1.

4.2 PROBABILITY DENSITY FUNCTION FOR CONTINUUM

Various studies suggest that a linear function is sufficient to describe the continuum BG in ΔE, so we use that for the ΔE PDF. For m_{ES} the standard PDF is the Argus function [9], and this proves

Table 1: Parameters used in the default ML fit. The parameters and their statistical errors are derived from MC studies described in the text. The signal ΔE PDF is proportional to $f_{core}\exp(\frac{-(\Delta E-\mu_{core})^2}{2\sigma^2_{core}}) + (1-f_{core})\exp(\frac{-(\Delta E-\mu_{tail})^2}{2\sigma^2_{tail}})$, the signal m_{ES} PDF is proportional to $\theta(\mu-m_{ES})\exp(\frac{-(m_{ES}-\mu)^2}{2\sigma^2_{left}}) + \theta(m_{ES}-\mu)\exp(\frac{-(m_{ES}-\mu)^2}{2\sigma^2_{right}})$, the continuum and non-peaking $B\overline{B}$ m_{ES} PDFs are proportional to $m_{ES}\sqrt{1-(\frac{m_{ES}}{m_0})^2}\exp(-\xi[1-(\frac{m_{ES}}{m_0})^2])$.

Fit component	Parameter	Value
Signal	ΔE μ_{core}	6.9 ± 0.2 MeV
	ΔE σ_{core}	14.3 ± 0.2 MeV
	ΔE μ_{tail}	2 ± 1 MeV
	ΔE σ_{tail}	37 ± 1 MeV
	ΔE f_{core}	$(85 \pm 1)\%$
	m_{ES} μ	5279.8 ± 0.1 MeV
	m_{ES} σ_{left}	2.8 ± 0.1 MeV
	m_{ES} σ_{right}	2.3 ± 0.1 MeV
Common BG	m_{ES} m_0	5289.8 MeV
Continuum BG	m_{ES} ξ	-17 ± 8
	ΔE linear slope	-1.9 ± 0.3
Non-peaking $B\overline{B}$ BG	m_{ES} ξ	-47 ± 24
	ΔE linear slope	-3.2 ± 0.6

sufficient. There is one parameter (the slope) for the ΔE PDF and two parameters (m_0 and ξ) for the Argus function. The parameters m_0 and ξ are correlated, and if the m_0 parameter is set too low, there can be problems with the fits. To avoid this problem, m_0 is fixed to 5.2898 GeV in the fit. It is, however, allowed to float when systematic errors are evaluated. Both the ΔE slope and ξ are floated in a fit to a continuum MC sample corresponding to 77 fb^{-1} of integrated luminosity. The projections of the MC events and the continuum BG PDFs are shown in Fig. 3. The values of the parameters used in these PDFs and in subsequent fits are shown in Table 1.

4.3 PROBABILITY DENSITY FUNCTION FOR NON-PEAKING $B\overline{B}$ BACKGROUND

The non-peaking $B\overline{B}$ BG has a similar source as the continuum BG (random combinations of real and fake K^0_s mesons) and so is expected to have a similar functional form. We used the same description (linear function for ΔE and Argus function for m_{ES}) as used for the continuum BG and fit them to $B\overline{B}$ MC samples with any candidates identified as signal or peaking $B\overline{B}$ BG removed. We used a m_0 parameter in common with the continuum BG, but the ΔE slope and Argus ξ parameter are allowed to float to different values from those used for continuum BG. The values determined by the fit to the non-peaking $B\overline{B}$ MC samples are also shown in Table 1.

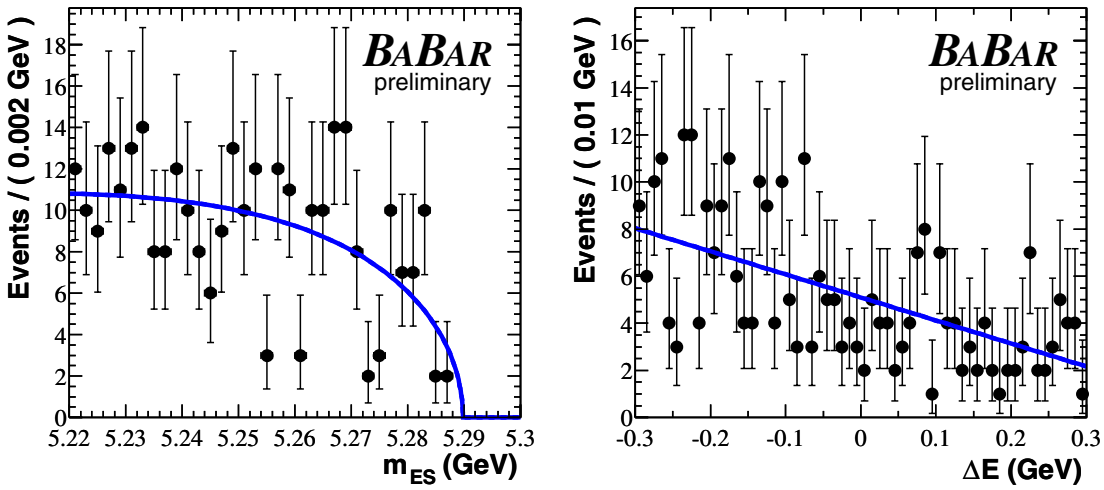

Figure 3: Distributions of m_{ES} and ΔE for selected candidates from $u\overline{u}/d\overline{d}/s\overline{s}/c\overline{c}$ MC simulated samples. The curves overlaid on the MC data points are the PDFs used to describe the continuum BG in the bounded $\Delta E - m_{ES}$ plane.

4.4 PROBABILITY DENSITY FUNCTION FOR PEAKING $B\overline{B}$ BACKGROUND

The distributions for the peaking $B\overline{B}$ BGs have a very different functional form from those for the continuum and non-peaking $B\overline{B}$ BGs. We have parametrized the peaking $B\overline{B}$ BG as was done in Ref. [10], by taking the two-dimensional (2D) histogram of all candidates (which pass the analysis cuts) from specially generated $B^0 \to 2K^0_s K^{*0}$ and $B^+ \to 2K^0_s K^{*+}$ MC samples and using this 2D histogram as the PDF.

The 2D histogram PDF, with the same binning used in the default fit, is shown in Fig. 4. By using a 2D histogram for the PDF, a large correlation between ΔE and m_{ES}, not present for the continuum or non-peaking $B\overline{B}$ BGs, is properly taken into account. Systematic errors due to the binned nature of this PDF are discussed later.

5 FIT FOR YIELD

We use the PDFs described in the preceding sections and the parameters derived from fits to MC samples and listed in Table 1 for our default fit to the on-resonance data sample. The values for the populations of the various components of the fit are

$$(N_S, N_{CBG}, N_{BNOP}, N_{BPBG}) = (71 \pm 9, 428^{+23}_{-29}, 0^{+26}_{-0}, 9 \pm 8).$$

The fit requires no $B\overline{B}$ non-peaking BG, but does allow for a small but not significant amount of $B\overline{B}$ peaking BG. The projections of the data and the fits on the m_{ES} and ΔE axes are shown in Fig. 5. The small contribution of the $B\overline{B}$ peaking BG is the non-overlap of the solid line (all components of the fit) and the dashed line (the continuum BG component of the fit) in the region $\Delta E < -0.10$ GeV in the ΔE plot.

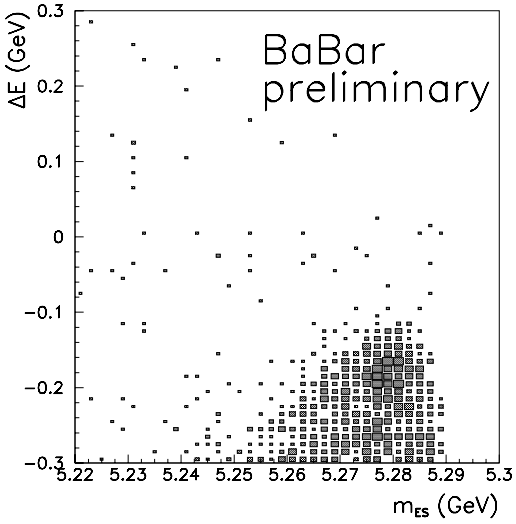

Figure 4: The two-dimensional histogram of ΔE vs. m_{ES} used as the PDF for the peaking $B\overline{B}$ BG.

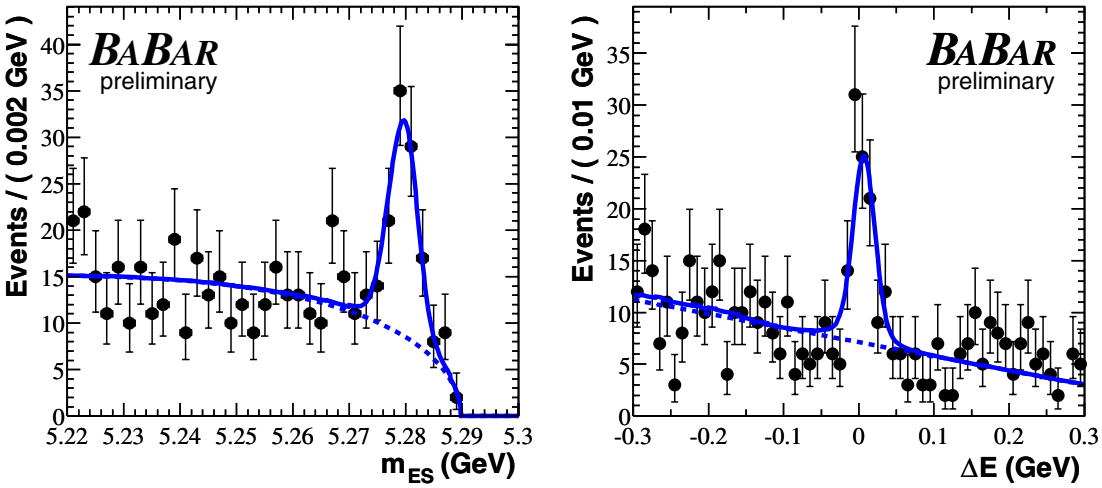

Figure 5: Distributions of m_{ES} and ΔE for selected candidates from the on-resonance data sample. The solid curve overlaid on the data corresponds to the sum of all PDFs, with their parameters (Table 1) and the signal and background fractions returned by the fit. The dashed curve is the contribution from the continuum BG.

6 SYSTEMATIC STUDIES

6.1 CUT-AND-COUNT ANALYSIS

We use a simple "cut-and-count" analysis to cross-check the results of the maximum likelihood fit, and to study several sources of systematic uncertainty. For the cut-and-count analysis we define

a signal region centered on the expected signal in $m_{\rm ES}$ and ΔE. The signal region is defined by $5.2704 < m_{ES} < 5.2884$ GeV and $-40 < \Delta E < +40$ MeV. We define two ΔE sidebands with the same $m_{\rm ES}$ cut but with $-300 < \Delta E < -100$ MeV and $+100 < \Delta E < +300$ MeV. The sum of the number of entries in the sidebands (57) scaled by the ratio of the area in the signal region to the area in the sidebands (0.2) gives an estimate of the number of BG events in the signal region (11 ± 2), where 78 events are observed, for a signal yield of 67 ± 9 events. The signal efficiency is slightly different between the cut-and-count analysis and the ML fit. The MC efficiency-corrected yield is 1295^{+170}_{-158} events for the ML fit and 1258 ± 169 events for the cut-and-count analysis. Given the different methods for estimating signal and background in the ML fit and the cut-and-count analysis, they are in reasonable agreement.

6.2 SIGNAL EFFICIENCY VARIATION ACROSS DALITZ PLOT

The cut-and-count analysis allows one to take all the entries in the signal region and plot the $m_{2K^0_s}$ distributions for these candidates, and compare them to those predicted by the reconstructed signal MC, which was generated with the assumption of non-resonance phase-space (uniform population of the Dalitz plot at generation). The distributions of the reconstructed $m_{2K^0_s}$ masses are consistent with (reconstructed) three-body phase space, but with such a small number of events in the data, we cannot rule out resonance production at the level of a few events per resonance in our data sample, or other small deviations from phase-space.

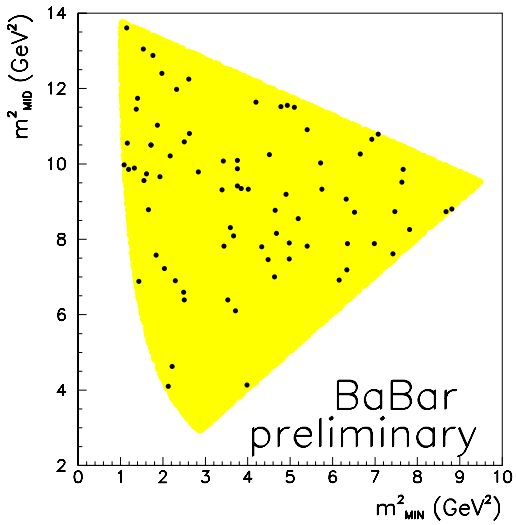

Figure 6: The folded Dalitz plot for the 78 candidates (black points) that pass the cut-and-count analysis and end up in the signal region. The signal/background for this selection is ~ 5.8. The yellow-shaded area is the physically-allowed region.

This is important because the efficiency calculated in different regions of the Dalitz plot is not uniform. It varies by more than a factor of two, mostly due to low efficiency for reconstructing K^0_s near some edges of the Dalitz plot. If the parent distribution for the data is the same as the MC parent distribution, this is not a problem, but since we do not know this, we need to assign a systematic error for the possibility that it is not.

We do this by dividing the "folded" Dalitz plot (one of the unique sextants of the $3K_s^0$ Dalitz plot) into 21 bins and calculating an efficiency for the cut-and-count analysis for each bin individually. The folded Dalitz plot we use is shown as the shaded area in Fig. 6; the points are the 78 candidates in the signal region of the cut-and-count analysis for the data. This folded Dalitz is achieved by ordering the three unique $m(2K_s^0)$ combinations for each $B^0 \to K_s^0 K_s^0 K_s^0$ candidate $m_{MAX}(2K_s^0) > m_{MID}(2K_s^0) > m_{MIN}(2K_s^0)$ and plotting $m_{MID}(2K_s^0)$ vs. $m_{MIN}(2K_s^0)$.

The entries in the signal region are then individually corrected for efficiency depending on what bin they populate, and the yield calculated this way is compared to the yield when all events are given the same (average) efficiency. The yield differs by 4.2% between the two ways of calculating the efficiency; we take this as the systematic error estimate due to a nonuniform population of the Dalitz plot.

6.3 K_s^0 RECONSTRUCTION EFFICIENCY

There is a small but well-measured disagreement between the $K_s^0 \to \pi^+\pi^-$ reconstruction efficiency in the data and the one reported by the full detector MC. We correct the efficiency and calculate a systematic error on how well we know the K_s^0 reconstruction efficiency. The efficiency in the MC simulation and data is measured as a function of K_s^0 transverse decay radius (r_{DEC}), transverse momentum and polar angle in the *BABAR* detector, and also for periods with different detector running conditions. A correction is calculated for each of the three K_s^0 candidates in a reconstructed MC event, and the product of the three correction factors (taken as the B^0 candidate correction factor) is averaged over all selected events in the signal MC sample. We do this for several different sets of measured efficiencies, each produced with different K_s^0 selection criteria. The corrections evaluated for different selection criteria are consistent, and the average correction factor is $\varepsilon_{data}/\varepsilon_{MC} = 0.950 \pm 0.014$.

The error includes a statistical error for the tables used to calculate the correction, a per-charged-track systematic error, and a per-K_s^0 systematic error. The quadrature sum of all these error estimates is 10.1%. This is the dominant source of systematic error for this measurement.

6.4 SIGNAL PARAMETRIZATION

We allow each of the eight parameters in the signal PDF to float in the fit, one at a time. The quadrature sum of the change in signal yield from these eight variations is 4.3%, and we take this as the systematic error estimate on our signal parametrization. Since many of the signal parameters are correlated, we also perform a fit where six of the signal parameters are free; only the ΔE tail-Gaussian mean and width are fixed to the values derived from the MC. The change in N_S from letting all these parameters float together is 2.4%. This is a variant of the above (larger) estimate that allows correlations between parameters to be taken into account, but we will use the larger estimate as a more conservative estimate.

6.5 BACKGROUND PARAMETRIZATION

As with the signal parameters, we allow each of the five BG PDF parameters to float in the fit, one at a time. For the binned-histogram peaking $B\overline{B}$ PDF, we increase and decrease the bin size by a factor of two and allow different levels of smoothing of the histogram. We take the largest of these variations as the systematic error due the peaking $B\overline{B}$ PDF, and add it in quadrature with the changes in signal yield from letting the BG fit parameters float. The fractional systematic error

estimated from all these variations is 0.8%. While the fit will not support all five BG parameters floating at once, we take the two parameters with the largest correlation (the ΔE slopes for the continuum and non-peaking $B\overline{B}$ BGs) and let them float together. The signal yield changes by 0.4%, less than the quadrature sum of the two parameters allowed to float separately. While the populations of the BG categories change noticeably with all these parameter variations, the total BG yield and the signal yield are quite stable.

6.6 FIT VALIDATION

We perform studies with parametrized MC simulations in which many samples of the same size (and category populations) as the data are generated from the PDFs. We also perform MC studies in which the background events are generated from the PDFs but the signal samples were extracted from the full-detector MC sample and fit along with the background samples. The means and uncertainties for the yields are all consistent with expectations, and no significant corrections for biases or systematic error contributions are required. For 2000 fitted toy MC samples, 48% have a larger value of $-\ln\mathcal{L}$ than that for the fit to the data.

There is a 15.9 fb^{-1} sample of data taken at CM energies just below the $\Upsilon(4S)$ resonance (the off-resonance data sample), which contains no B-meson decays. This data is corrected for a shift in the $m_{\rm ES}$ endpoint due to different beam energies. The data is subjected to the same selection cuts and the same ML fit as the on-resonance data. The signal yield from this fit is consistent with zero events.

6.7 OTHER FIT VARIATIONS

As a measure of the sensitivity to background parameterizations, we remove the three BG categories one at a time in our default ML fit. With either (or both) of the $B\overline{B}$ BG PDFs removed, the yield changes by very little ($< 0.3\%$). With the continuum BG PDF removed, the signal yield changed noticeably (-5.1%), but the likelihood of the no-continuum-BG fit is much worse than that for the default fit. That is, neither of the $B\overline{B}$ BGs (or their combination) does a particularly good job of describing the continuum BG, which dominates the bounded ΔE-$m_{\rm ES}$ plane away from the signal region.

We remove the restriction that each of the four yields be greater than zero and refit. The signal yield changes by $+1.3\%$, and the likelihood of this fit is only slightly better.

We add (separately) quadratic terms to the continuum and non-peaking $B\overline{B}$ ΔE PDFs and let them float in the fit; the signal yield changes by -2.2% and -0.6%. We include these variations in the systematic uncertainty along with the other systematic errors estimated from floating the background parameters above.

6.8 CANDIDATE SELECTION CRITERIA

While the candidate selection cuts listed in Section 3 are quite standard and we expect the MC to reproduce them, we estimate a systematic error on each one to account for the fact that the MC might not exactly reproduce the data. Where possible, each cut is removed in turn and the change in yield for the data is compared with that for the MC. For the few cuts that are significantly correlated, both cuts are removed at the same time. The cuts are also tightened by reasonable amounts and the change in yield in the data and MC are compared. Various other studies are performed on control channels such as $B^0 \to D^{*-}\pi^+$, $D^{*-} \to \pi_s^-\overline{D}^0$, $\overline{D}^0 \to K^0_s\pi^+\pi^-$, which has a

similar topology and a large enough branching fraction so that it can be reconstructed with minimal cuts. The quadrature sum of the systematic error estimated from a variation for each cut is 5.0%, where the dominant contributions are from the $\Delta m_{\pi^+\pi^-}$ cut (3.0%), the $\cos\theta_T$ cut (2.5%), and the R_2 cut (2.1%).

6.9 SYSTEMATIC ERROR SUMMARY

There are two other small systematic errors shown in Table 2 not discussed above: the statistical error on the MC used to derive the signal efficiency estimate, and the error on the total number of $B\overline{B}$ pairs in our data sample. With these added in quadrature with the systematic error estimates described above, the total (fractional) systematic error is 13.1%.

Table 2: Summary of fractional systematic uncertainties.

Source	Estimated from	Percent Error
K_s^0 efficiency	detector studies	10.1%
BG Parametrization	vary in fit	2.4%
Signal Parametrization	vary in fit	4.3%
Candidate Selection Cuts	cut variations, studies	5.0%
Efficiency variation	cut-and-count analysis	4.2%
Signal efficiency	MC statistics	1.3%
$B\overline{B}$ counting		1.1%
Total		13.1%

7 PHYSICS RESULTS

The branching fraction is calculated from the relationship $\mathcal{B} = N_S/(\varepsilon N_{B\overline{B}})$, where $N_S = 71 \pm 9$ is the signal yield from the fit, and ε is the product of $\varepsilon_{MC} = 5.50\%$ derived from the signal MC and $\varepsilon_{data}/\varepsilon_{MC} = 95.0\%$, derived from the K_s^0 efficiency studies. These combine for an efficiency-corrected signal yield of 1363^{+179}_{-167}. The data set corresponds to 211×10^6 B^0 and $\overline{B^0}$ decays, and we calculate $\mathcal{B} = (6.5 \pm 0.8) \times 10^{-6}$ (statistical error only). We assume that the rate for $B^0\overline{B^0}$ and B^+B^- production in $\Upsilon(4S)$ decays is equal. The errors on all quantities except for the signal yield are included in the systematic error estimate. If we fix the signal yield to zero in our ML fit, the difference between the $-\ln\mathcal{L}$ of this fit and the default fit gives a statistical significance for our observation of 15.6σ.

The sum of the systematic error estimates is given in Table 2. This results in a measurement of $\mathcal{B} = (6.5 \pm 0.8 \pm 0.8) \times 10^{-6}$, where the second error is the systematic error estimate. One sigma of the total systematic error estimate (not just the ones that pertain to the signal yield) corresponds to 9.3 (efficiency-uncorrected) events. When the signal yield is fixed to 9.3 and the data is refit, the change in $-\ln\mathcal{L}$ from the default fit corresponds to a significance of 10.9σ.

We note that this measurement is consistent with the previous Belle measurement, but by itself it is more than 2σ above the prediction made using $\mathcal{B}(B^+ \to K^+K^-K^+)$ and the assumption of penguin dominance in $B \to KKK$. However, if this difference is confirmed with more data, it may

just be evidence of resonant intermediate states occurring at different rates in $B^0 \to K^0_s K^0_s K^0_s$ and ($\phi-$removed) $B^+ \to K^+K^-K^+$.

While we have examined the folded Dalitz plot for the cut-and-count analysis and see nothing that looks like a narrow resonance (broad resonances cannot be ruled out given the size of the data sample), decays like $B^0 \to \chi_{c0}K^0$ may be present and are clearly not part of the relationship between $B^0 \to K^0_s K^0_s K^0_s$ and $B^+ \to K^+K^-K^+$. To estimate the amount of this type of decay in our sample, we reject $2K^0_s$ masses within ± 50 MeV (about 3σ of our resolution) of the χ_{c0} and χ_{c2} masses. We apply this rejection to the data and the MC samples in our cut-and-count analysis and, while a few entries are removed from the data, proportionally slightly more were removed from the non-resonant phase-space generated MC, so the efficiency-corrected yield goes *up* slightly (consistent with no change) when the χ_c bands are excluded. On the basis of this, we cannot claim we observe any contribution to the $B^0 \to K^0_s K^0_s K^0_s$ signal from $B^0 \to \chi_c K^0$, and so we leave the inclusive measurement uncorrected.

8 SUMMARY

From a sample of 211×10^6 $B\overline{B}$ decays recorded with the *BABAR* detector, we observe a signal of 71 ± 9 $B^0 \to K^0_s K^0_s K^0_s$ decays, and with these measure a branching fraction $\mathcal{B}(B^0 \to K^0_s K^0_s K^0_s) = (6.5 \pm 0.8 \pm 0.8) \times 10^{-6}$. This result is preliminary.

9 ACKNOWLEDGMENTS

We are grateful for the extraordinary contributions of our PEP-II colleagues in achieving the excellent luminosity and machine conditions that have made this work possible. The success of this project also relies critically on the expertise and dedication of the computing organizations that support *BABAR*. The collaborating institutions wish to thank SLAC for its support and the kind hospitality extended to them. This work is supported by the US Department of Energy and National Science Foundation, the Natural Sciences and Engineering Research Council (Canada), Institute of High Energy Physics (China), the Commissariat à l'Energie Atomique and Institut National de Physique Nucléaire et de Physique des Particules (France), the Bundesministerium für Bildung und Forschung and Deutsche Forschungsgemeinschaft (Germany), the Istituto Nazionale di Fisica Nucleare (Italy), the Foundation for Fundamental Research on Matter (The Netherlands), the Research Council of Norway, the Ministry of Science and Technology of the Russian Federation, and the Particle Physics and Astronomy Research Council (United Kingdom). Individuals have received support from CONACyT (Mexico), the A. P. Sloan Foundation, the Research Corporation, and the Alexander von Humboldt Foundation.

References

[1] M. Gronau and J. L. Rosner, Phys. Lett. B 564, 90 (2003).

[2] The Heavy Flavor Averaging Group, http://www.slac.stanford.edu/xorg/hfag/rare/pre_winter04/charmless/index.html

[3] The Belle Collaboration, A. Garmash *et al.,* Phys. Rev. D **69**, 012001 (2004).

[4] Particle Data Group, K. Hagiwara *et al.*, Phys. Rev. **D66**, 010001 (2002).

[5] The *BABAR* Collaboration, B. Aubert *et al.*, Nucl. Instrum. Methods **A479**, 1 (2002).

[6] The GEANT4 Collaboration, S. Agostini *et al.*, Nucl. Instrum. Methods **A506**, 250 (2003).

[7] R. A. Fisher, Annals Eugen. **7**, 179 (1936).

[8] G. C. Fox and S. Wolfram, Phys. Rev. Lett. **41**, 1581 (1978).

[9] The Argus Collaboration, H. Albrecht *et al.,* Z.Phys. C48, 543 (1990).

[10] The *BABAR* Collaboration, B. Aubert *et al.*, arXiv:hep/ex-0406005, submitted to Phys. Rev. Lett.